High-order harmonic generation by bi-elliptical orthogonally polarized two-color fields

D. B. Milošević [1,2,3,*] and W. Becker [3,4]

[1]*Faculty of Science, University of Sarajevo, Zmaja od Bosne 35, 71000 Sarajevo, Bosnia and Herzegovina*
[2]*Academy of Sciences and Arts of Bosnia and Herzegovina, Bistrik 7, 71000 Sarajevo, Bosnia and Herzegovina*
[3]*Max-Born-Institut, Max-Born-Strasse 2a, 12489 Berlin, Germany*
[4]*National Research Nuclear University MEPhI, Kashirskoe Shosse 31, 115409 Moscow, Russia*

(Received 4 May 2020; revised 9 July 2020; accepted 23 July 2020; published 10 August 2020)

Based on the strong-field approximation, we report results for high-order harmonic generation by bi-elliptical orthogonally polarized two-color (BEOTC) fields with frequency ratios of 2:1 and 3:1 and fundamental wavelengths of 800 and 1800 nm. A BEOTC field denotes the superposition of two copropagating counter-rotating elliptically polarized fields with different wavelengths and orthogonal semimajor axes. Its two limiting cases are the bicircular field and the linearly polarized orthogonal two-color field [D. B. Milošević and W. Becker, Phys. Rev. A **100**, 031401(R) (2019)]. A detailed analysis of the high-order harmonic intensities and ellipticities as functions of the harmonic order, the ellipticity, and the relative phase between the two driving-field components is presented. Regions of the parameter space are identified where the harmonic ellipticities are very high. Surprisingly, this can be the case already for very small ellipticity (as small as $\varepsilon = 0.01$) of the driving field. This can be important for practical applications. In the opposite limit where the BEOTC field is close to bicircular, the selection rules that govern the latter case can also be very quickly invalidated. For the 2:1 case, this can result in an apparent shift of the selection rules by one harmonic order.

DOI: 10.1103/PhysRevA.102.023107

I. INTRODUCTION

High-order harmonic generation (HHG) is in a position to bridge the gap in intensity and frequency between x rays provided by free-electron-laser (FEL)-based sources and more traditional nonlinear-optics sources. HHG proceeds via ionization of an atom (or molecule) by an intense laser pulse. The liberated electron collects energy from the laser field, which it emits in the form of a single photon when it is driven into a recollision with its parent atom. In the past, linearly polarized monochromatic laser pulses have been used for this purpose, which generate linearly polarized harmonics with a frequency spectrum that is almost flat up to a certain cutoff frequency where it terminates rather abruptly. However, for many applications, x rays with circular or elliptical polarizations are desirable. In particular, the case of circular polarization is important since using such harmonics it is possible to analyze and, possibly, discriminate the enantiomers of a chiral molecule. Many biomolecules exhibit circular dichroism [1–10]. In addition, such harmonics can be used to analyze the magnetic structure of materials (so-called x-ray magnetic circular dichroism [11–19]).

Initially, the process of HHG did not seem to lend itself to producing circularly polarized harmonics. Namely, a circularly polarized laser pulse does not generate any harmonics while a field with elliptical polarization does produce elliptically polarized harmonics, but with rather low yield as soon as the driving ellipticity is substantially different from zero. The limitations inherent in a linearly polarized driving pulse can be overcome by using "tailored" fields, which are custom made according to the experimenters' requirements and subject to their technical capabilities. Especially, superpositions of two fields with different frequencies and polarizations (and, sometimes, propagation directions) have been employed. Bicircular fields, viz., superpositions of two copropagating fields with counter-rotating circular polarization and a frequency ratio of typically, though not necessarily, 2:1, have become popular because they generate circularly polarized harmonics with helicities alternating between 1 and -1 from one harmonic to the next. More information about bicircular fields can be found in Refs. [20–30]. Two copropagating orthogonal linearly polarized fields with different frequencies [an orthogonal two-color (OTC) field] generate very interesting harmonics: for a frequency ratio of 2:1, the harmonics are linearly polarized in the direction of either driving component while for a frequency ratio of 3:1, they are elliptically polarized. The frequency spectrum can also be very different from the standard shape of a plateau with a well-defined cutoff, as it is familiar from linear polarization. Depending on the various parameters (component intensities, frequencies, and relative phase), there may be a very pronounced cutoff or no cutoff at all, and the spectrum can have just about any shape in place of the plateau. In Ref. [31] we have shown that with the ω-3ω OTC field it is possible to generate elliptically polarized harmonics with energies much higher than can be generated by a bicircular field for the same driving-pulse intensities.

OTC fields have attracted interest and have been theoretically investigated and experimentally utilized for various purposes for a long time already [20,21,32–65]. In one of the earlier applications, HHG was very efficiently enhanced by the addition to the fundamental driving field of a stronger [33,34] or weaker [35] orthogonally polarized second

*Corresponding author: milo@bih.net.ba

harmonic. A very general motivation to superimpose a second harmonic is the following: The two half cycles of a linearly polarized driving field are equivalent insomuch as HHG is concerned. This symmetry prohibits one from extracting subcycle information from a harmonic spectrum. The symmetry is broken by the presence of a second-order (or higher) harmonic which, moreover, introduces the relative phase as an additional control parameter. If the harmonic is perpendicular to the fundamental, i.e., for an OTC field, the dynamics unfold in a plane, which can be exploited to yield additional information. This is the basic reason why OTC fields have become important. For example, it becomes possible to select and/or to affect a specific quantum trajectory [36–42], to enhance individual harmonics [43–45], to extract the ionization time [46], or to explore atomic wave functions or cross sections or molecular orbitals [38,47–54], the pertinent selection rules for the emitted harmonics [55], or the molecular-orientation dependence [56]. Polarization control of the harmonics is about to be explored [57–59].

In the present paper we analyze HHG by a "bi-elliptical" orthogonal two-color (BEOTC) field, viz., two copropagating elliptically polarized fields with their major polarization axes at right angles to each other. BEOTC fields have so far only received little attention [54,66–68]. For the component ellipticities $\varepsilon_1 = \varepsilon_2 = 1$ this field reduces to the bicircular field, while for $\varepsilon_1 = \varepsilon_2 = 0$ it becomes the OTC field. Our formalism allows for an arbitrary integer frequency ratio of s:r, but in the specific examples we restrict ourselves to ratios of 2:1 or 3:1. For the OTC fields, these two configurations generate very different harmonics as mentioned above.

In Sec. II we define our BEOTC field, introduce the observables which we calculate, such as the harmonic intensities and polarizations, and derive the selection rules. Our numerical results are presented in Sec. III and the conclusions are given in Sec. IV. Atomic units are used throughout.

II. THEORY

A. Definition of the BEOTC field

We consider the BEOTC field, which consists of an elliptical field of frequency $r\omega$, amplitude E_1, and ellipticity ε_1 with the x axis as the major axis and a second coplanar elliptical field of frequency $s\omega$, amplitude E_2, and ellipticity ε_2 with the y axis as the major axis. The period of the fundamental frequency is $T = 2\pi/\omega$. The electric-field vector of this field is $\mathbf{E}(t) = \mathbf{E}_1(t) + \mathbf{E}_2(t)$ with

$$\mathbf{E}_1(t) = \frac{E_1}{\sqrt{1+\varepsilon_1^2}}[\hat{\mathbf{e}}_x \sin(r\omega t) - \varepsilon_1 \hat{\mathbf{e}}_y \cos(r\omega t)] = \frac{i}{2} E_1 \frac{\hat{\mathbf{e}}_x + i\varepsilon_1 \hat{\mathbf{e}}_y}{\sqrt{1+\varepsilon_1^2}} e^{-ir\omega t} + \text{c.c.}, \quad (1)$$

$$\mathbf{E}_2(t) = \frac{E_2}{\sqrt{1+\varepsilon_2^2}}[\hat{\mathbf{e}}_y \sin(s\omega t + \phi) - \varepsilon_2 \hat{\mathbf{e}}_x \cos(s\omega t + \phi)] = \frac{i}{2} E_2 \frac{\hat{\mathbf{e}}_y + i\varepsilon_2 \hat{\mathbf{e}}_x}{\sqrt{1+\varepsilon_2^2}} e^{-i(s\omega t+\phi)} + \text{c.c.}, \quad (2)$$

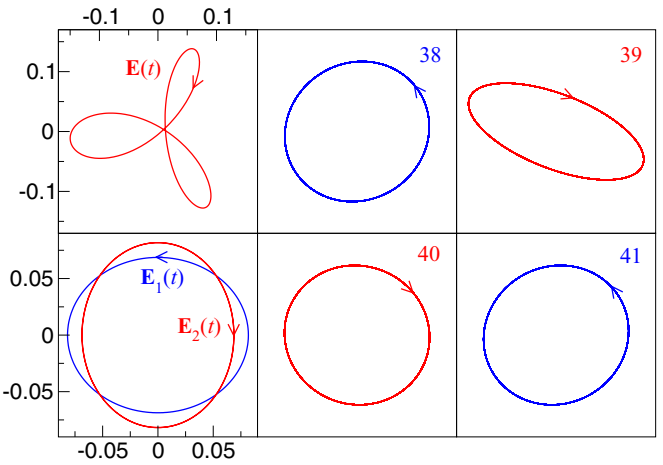

FIG. 1. Left: BEOTC field $\mathbf{E}(t)$ (upper) and its components $\mathbf{E}_1(t)$ and $\mathbf{E}_2(t)$ (lower) for the ω-2ω field with ellipticities $\varepsilon_1 = \varepsilon_2 = 0.84$, the relative phase $\phi = 0.92\pi$, and the field component intensities $I_1 = I_2 = 4 \times 10^{14}$ W/cm^2. Middle and right: Fields of the harmonics $n = 38$, 39, 40, and 41, generated by He atoms exposed to the BEOTC field.

where $\hat{\mathbf{e}}_x$ and $\hat{\mathbf{e}}_y$ are real unit vectors, which span the xy plane, and ϕ is the relative phase between the two components. For $\varepsilon_1 = \varepsilon_2 = \varepsilon$, the field components are counter-rotating in the xy plane. For $\varepsilon_1 = \varepsilon_2 = 0$, this field reduces to the OTC field (see Ref. [31] and references therein), while for $\varepsilon_1 = \varepsilon_2 = 1$ it becomes the bicircular field [23,24,26,29]. An example of the ω-2ω BEOTC field is shown in the upper left panel of Fig. 1. The electric-field vectors of the two components are shown in the lower left panel. In the remaining panels we show the harmonic fields for $n = 38$, 39, 40, and 41 (see Sec. III C for explanations; these examples do not obey the known selection rule for HHG by bicircular field, according to which the harmonic $n = 39$ is forbidden).

The BEOTC field can be rewritten as a sum of two bicircular fields, $\mathbf{E}(t) = \mathbf{E}_1^{\text{bc}}(t) + \mathbf{E}_2^{\text{bc}}(t)$, where

$$\mathbf{E}_1^{\text{bc}}(t) = \frac{i}{2}\left[\frac{E_1(1+\varepsilon_1)}{\sqrt{2(1+\varepsilon_1^2)}}\hat{\mathbf{e}}_+ e^{-ir\omega t} + \frac{E_2(1+\varepsilon_2)}{\sqrt{2(1+\varepsilon_2^2)}}\hat{\mathbf{e}}_- e^{-i(s\omega t+\phi-\pi/2)}\right] + \text{c.c.}, \quad (3)$$

$$\mathbf{E}_2^{\text{bc}}(t) = \frac{i}{2}\left[\frac{E_2(\varepsilon_2-1)}{\sqrt{2(1+\varepsilon_2^2)}}\hat{\mathbf{e}}_+ e^{-i(s\omega t+\phi-\pi/2)} + \frac{E_1(1-\varepsilon_1)}{\sqrt{2(1+\varepsilon_1^2)}}\hat{\mathbf{e}}_- e^{-ir\omega t}\right] + \text{c.c.}, \quad (4)$$

with $\hat{\mathbf{e}}_\pm = (\hat{\mathbf{e}}_x \pm i\hat{\mathbf{e}}_y)/\sqrt{2}$ [69]. Therefore, the BEOTC field is a sum of two pairs of counter-rotating circularly polarized fields, and high-order harmonic generation by this field can be analyzed similarly as in Ref. [26].

B. Harmonic intensity and ellipticity

The nth-harmonic intensity (power) P_n and ellipticity ε_n for the laser field given by Eqs. (1)–(4) are defined by (in atomic units; see Ref. [26] and references therein)

$$P_n = \frac{(n\omega)^4}{2\pi c^3}|T_n|^2, \tag{5}$$

$$\varepsilon_n = \mathrm{sgn}(\xi_n)\left(\frac{1-\sqrt{1-\xi_n^2}}{1+\sqrt{1-\xi_n^2}}\right)^{1/2}, \tag{6}$$

with the degree of circular polarization $\xi_n = \mathrm{Im}\,(2T_{nx}^* T_{ny})/|T_n|^2$. The vector $\mathbf{T}_n = \int_0^T dt\mathbf{d}(t)e^{in\omega t}/T$ is defined as the Fourier component of the time-dependent dipole $\mathbf{d}(t) = \sum_a \mathbf{d}_a(t)$, where the sum is over all possible values a of the atomic ground-state quantum number (the quantum-mechanical method of the calculation of $\mathbf{d}_a(t)$, based on the strong-field approximation, is described in Ref. [29]). The vector $\mathbf{T}_n$ can be written as $\mathbf{T}_n = |T_n|\mathbf{e}_n = T_{nx}\hat{\mathbf{e}}_x + T_{ny}\hat{\mathbf{e}}_y = T_{n+}\hat{\mathbf{e}}_+ + T_{n-}\hat{\mathbf{e}}_-$, with $\mathbf{e}_n$ the complex unit polarization vector of the nth harmonic, $|T_n| = \mathbf{e}_n^* \cdot \mathbf{T}_n$, and $\xi_n = 2\varepsilon_n/(1+\varepsilon_n^2) = i\hat{\mathbf{k}}\cdot(\hat{\mathbf{e}}_n \times \hat{\mathbf{e}}_n^*) = (|T_{n+}|^2 - |T_{n-}|^2)/(|T_{n+}|^2 + |T_{n-}|^2)$ $(-1 \leqslant \xi_n \leqslant 1)$, with $\hat{\mathbf{k}} = \mathbf{k}/|\mathbf{k}|$ ($\mathbf{k}$ being the wave vector) the unit vector along the z axis. The components with helicities $+1$ and -1, T_{n+} and T_{n-}, respectively, contribute coherently to the HHG process and, in general, elliptically polarized harmonics are emitted. The nth-harmonic polarization ellipse is rotated by an offset angle θ_n with respect to the polarization ellipse defined by $\hat{\mathbf{e}}_x$ and $\hat{\mathbf{e}}_y$ [23]. The offset angle is determined by the relation

$$\theta_n = \mathrm{Im}\left\{\ln\left[\sqrt{1+\varepsilon_n^2}(\mathrm{Re}\,T_{nx} + i\mathrm{Re}\,T_{ny})/|T_n|\right]\right\}. \tag{7}$$

This is different from the formulas in Refs. [23,70] where inverse trigonometric functions were used to express $2\theta_n$.

The complex time-dependent nth-harmonic electric-field vector is [24,29] $\mathbf{E}_n(t) = n^2|T_n|\mathbf{e}_n e^{-in\omega t}$, with

$$\mathbf{e}_n = \frac{1+\varepsilon_n}{\sqrt{2(1+\varepsilon_n^2)}}e^{-i\theta_n}\hat{\mathbf{e}}_+ + \frac{1-\varepsilon_n}{\sqrt{2(1+\varepsilon_n^2)}}e^{i\theta_n}\hat{\mathbf{e}}_-. \tag{8}$$

The nth-harmonic polarization vector can be written as $\mathbf{e}_n = (\hat{\mathbf{e}}_{nx} + i\varepsilon_n\hat{\mathbf{e}}_{ny})/\sqrt{1+\varepsilon_n^2}$, where the harmonic ellipticity ε_n and the real orthogonal unit vectors $\hat{\mathbf{e}}_{nx}$ and $\hat{\mathbf{e}}_{ny}$ determine the orientation of the harmonic-field polarization ellipse, which is rotated by the angle θ_n with respect to the laser-field polarization ellipse (i.e., with respect to the x axis). The unit vectors $\hat{\mathbf{e}}_{n\pm} = (\hat{\mathbf{e}}_{nx} \pm i\hat{\mathbf{e}}_{ny})/\sqrt{2}$ in the rotated coordinate system, which are connected with the nth-harmonic polarization ellipse, satisfy the relation $\hat{\mathbf{e}}_{n\pm} = \exp(\mp i\theta_n)\hat{\mathbf{e}}_\pm$.

C. Selection rules

In the HHG process integer numbers $p_\pm$ ($q_\pm$) of photons are exchanged with the field component having frequency $r\omega$ ($s\omega$) and helicity ± 1, so that the energy-conserving condition for the nth harmonic is

$$n\omega = (p_+ + p_-)r\omega + (q_+ + q_-)s\omega. \tag{9}$$

The projection of the total angular momentum on the z axis is conserved. Having in mind that each absorbed photon from the field component proportional to $\hat{\mathbf{e}}_\pm$ in Eqs. (3) and (4) changes the angular momentum projection by ± 1 and that the emitted nth-harmonic component proportional to $\hat{\mathbf{e}}_\pm$ in Eq. (8) changes this projection by ∓ 1, the condition that the angular momentum projection be conserved takes the form

$$p_+ - p_- + q_+ - q_- \mp 1 = 0, \tag{10}$$

where ∓ 1 stands for the emission of a circularly polarized nth harmonic with helicity ∓ 1. This implies that the total number $p_+ + p_- + q_+ + q_-$ of photons exchanged with the field is odd as required by parity conservation. Introducing $p_+ = p_- - q_+ + q_- \pm 1$ into Eq. (9) we obtain the following selection rule for the $T_{n\pm}$ component of the T-matrix element:

$$n_\pm = (2p_- + q_- - q_+ \pm 1)r + (q_- + q_+)s. \tag{11}$$

The nth harmonic has contributions of $T_{n=n_+}$ and $T_{n=n_-}$ components which add coherently and, therefore, produce an elliptically polarized nth harmonic. For the ω-3ω field, Eq. (11) reduces to

$$r = 1, \quad s = 3, \quad n_\pm = 2(p_- + 2q_- + q_+) \pm 1, \tag{12}$$

so that only odd elliptically polarized high-order harmonics are emitted. This can also be shown taking into account that for r and s odd we have $\mathbf{E}(t + T/2) = -\mathbf{E}(t)$ and $\mathbf{d}(t + T/2) = -\mathbf{d}(t)$ so that $\mathbf{T}_n = \int_0^{T/2} dt\mathbf{d}(t)e^{in\omega t}(1 - e^{in\pi})/T$, which is different from zero only for n odd.

III. NUMERICAL RESULTS

A. Results for the ω-3ω BEOTC field and 1800 nm

Let us now present numerical results for HHG by a He atom exposed to a BEOTC field. We choose the fundamental wavelength of 1800 nm, while the field component ellipticities and intensities are equal: $\varepsilon_1 = \varepsilon_2 = \varepsilon$ and $E_1^2 = E_2^2 = 5 \times 10^{14}$ W/cm^2.

We first present results for the ω-3ω BEOTC field in Figs. 2–4. As mentioned above, only odd harmonics are emitted. In addition, for $(\varepsilon, \phi) \to (-\varepsilon, \phi + \pi)$ from Eqs. (1) and (2) it follows that $E_x(t) \to E_x(t)$ and $E_y(t) \to -E_y(t)$. Taking into account the explicit form of the matrix elements for the He atom, we obtain that in this case $T_{nx} \to T_{nx}$ and $T_{ny} \to -T_{ny}$ so that $P_n \to P_n$ and $\varepsilon_n \to -\varepsilon_n$. Therefore, a simultaneous change of the sign of the ellipticity and a shift of the relative phase by π does not change the harmonic intensity, while the harmonic ellipticity changes its sign. Hence, it is enough to calculate P_n and ε_n for positive ε and $\phi \in [0, 2\pi]$, as presented in Figs. 2–4. Then the results for $-\varepsilon$ and phase ϕ are obtained from the results calculated for ε and $\phi + \pi$.

The upper panels of Fig. 2 confirm that for $\varepsilon = 0$, which corresponds to the OTC field considered in Ref. [31], upon $\phi \to \phi + \pi$ the harmonic intensity is invariant while the harmonic ellipticity changes its sign. The results obtained are qualitatively similar to those presented in Ref. [31]. In addition to the conclusions drawn in Ref. [31], we see that for low harmonic order ($n < 200$) the ellipticity of the harmonics can be very high for suitable relative phases. This result was not discussed in Ref. [31] and we analyze it in more detail in the next section where a similar effect is observed for the ω-2ω BEOTC field for very low ellipticities. We should

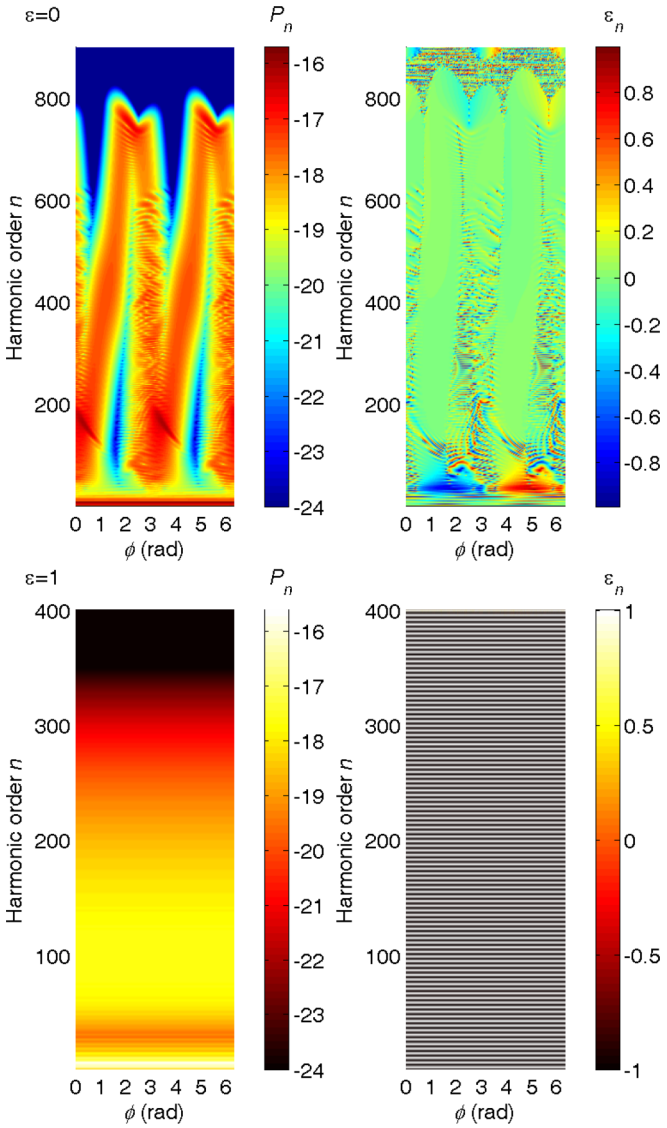

FIG. 2. Logarithm of the harmonic intensity P_n (left) and ellipticity ε_n (right) for HHG by He atoms, presented in false colors as functions of the relative phase between the ω-3ω BEOTC field components ϕ (abscissa) and the harmonic order n (ordinate). The BEOTC field component ellipticities are equal $\varepsilon_1 = \varepsilon_2 = \varepsilon$, component intensities are $E_1^2 = E_2^2 = 5 \times 10^{14}$ W/cm^2, and the fundamental wavelength is 1800 nm. Top: $\varepsilon = 0$ (OTC field). Bottom: $\varepsilon = 1$ (bicircular field).

also emphasize the extremely strong dependence of the shape of the harmonic spectrum on the relative phase ϕ (note the logarithmic color code).

In the lower panels of Fig. 2 we present the same results for the opposite limit, namely, the bicircular field [$\varepsilon = 1$, $\mathbf{E}_2(t) = \mathbf{0}$]. The cutoff is much lower than in the OTC field case and the results do not depend on the relative phase. Since $q_+ = p_- = 0$ in Eq. (12), only the harmonics $n_\pm = 4q_- \pm 1$ having helicity ± 1 are emitted.

Figure 3 illustrates how the harmonic intensity and ellipticity change when the BEOTC ellipticity increases from $\varepsilon = 0.1$ to $\varepsilon = 0.6$. The first observation is that the invariance upon $\phi \to \phi + \pi$ is lost. For a broad interval of relative phases the cutoff of the spectrum remains very high (near $n = 800$), even for ellipticities as high as $\varepsilon = 0.5$, but the yield P_n falls off quickly as soon as $\varepsilon \geqslant 0.4$. We also notice regions in which the harmonic ellipticity is high, in particular for low harmonic orders. The corresponding results for the BEOTC field ellipticities $\varepsilon = 0.7, 0.8, 0.9$ are presented in Fig. 4. The cutoff is lower. Interesting sickle-like regions occur in the (n, ϕ) plane in which the harmonic ellipticity changes quickly from $\varepsilon_n = 1$ to $\varepsilon_n = -1$. In these regions, the alternating helicities for the bicircular field are already anticipated (lower right panel of Fig. 2).

B. Results for the ω-2ω BEOTC field and 1800 nm

In Figs. 5–11 we present numerical results for the ω-2ω BEOTC field. In this case, both even and odd harmonics of the fundamental frequency are emitted. The results are invariant with respect to a shift of the relative phase by π, $\phi \to \phi + \pi$. The reason is that the field component $\mathbf{E}_1(t)$ does not depend on ϕ, while the component $\mathbf{E}_2(t)$ changes sign for the shift of ϕ by π. On the other hand, the field component $\mathbf{E}_1(t)$ changes sign for $t \to t + T/2$, while the component $\mathbf{E}_2(t)$ remains unchanged. Therefore, for $\phi \to \phi + \pi$ and $t \to t + T/2$ both $\mathbf{E}_1(t)$ and $\mathbf{E}_2(t)$ change sign, which means that both T_{nx} and T_{ny} change sign so that P_n and ε_n remain unchanged. For $\varepsilon \to -\varepsilon$ the x component of $\mathbf{E}_1(t)$ remains unchanged, while the y component changes sign. The opposite is valid for the $\mathbf{E}_2(t)$ component. Therefore, the harmonic intensity is invariant with respect to a change of sign of the ellipticity, while the harmonic ellipticity ε_n changes sign for $\varepsilon \to -\varepsilon$, since $\mathrm{sgn}(\varepsilon_n) = \mathrm{sgn}[\mathrm{Im}\,(2T_{nx}^* T_{ny})]$ according to Eq. (6).

For the ω-2ω OTC field ($\varepsilon = 0$) the harmonic ellipticity is $\varepsilon_n = 0$, while for the ω-2ω bicircular field ($\varepsilon = 1$) the harmonic ellipticities are $\varepsilon_{n_\pm} = \pm 1$ for the harmonic order $n_\pm = 3q_- \pm 1$. Therefore, in Fig. 5 we present only the harmonic intensities. For the bicircular field (right panel), the harmonic intensity does not depend on the relative phase and the cutoff is much lower than for the OTC field (left panel). For the OTC field (left panel), remarkably, there is a region of the relative phase around $\phi = 2.2$ rad with practically no harmonic emission at all.

In Fig. 6 we present both the harmonic intensity and the harmonic ellipticity for ellipticities $\varepsilon = 0.1, \ldots, 0.6$. The cutoff for the ω-2ω BEOTC field is higher than that of the ω-3ω case and remains above $n = 800$ for all ellipticities $\varepsilon \leqslant 0.5$. As in the ω-3ω case, there are regions in which the harmonic ellipticity is high. This is particularly pronounced for low harmonic orders. As mentioned, the harmonic ellipticity is zero for $\varepsilon = 0$. Therefore, it is surprising that upon the small change from $\varepsilon = 0.0$ to $\varepsilon = 0.1$ the harmonic ellipticity can be high; consider, for example, the region near $\phi = 0$ and $n < 500$ or the region below $n = 100$ for a wide interval of ϕ (this case is analyzed in more detail below) in the right subpanel of the upper left panel. Finally, in Fig. 7 we present the corresponding results for the ellipticities $\varepsilon = 0.7, 0.8, 0.9$. The high-harmonic cutoff is below $n = 700$ and regions of high harmonic ellipticity can be noticed, similarly as in the ω-3ω case.

Figure 6 demonstrates that the magnitude of the harmonic ellipticity can be very high for low harmonic orders (around $n = 50$) even though the BEOTC field ellipticity is very low

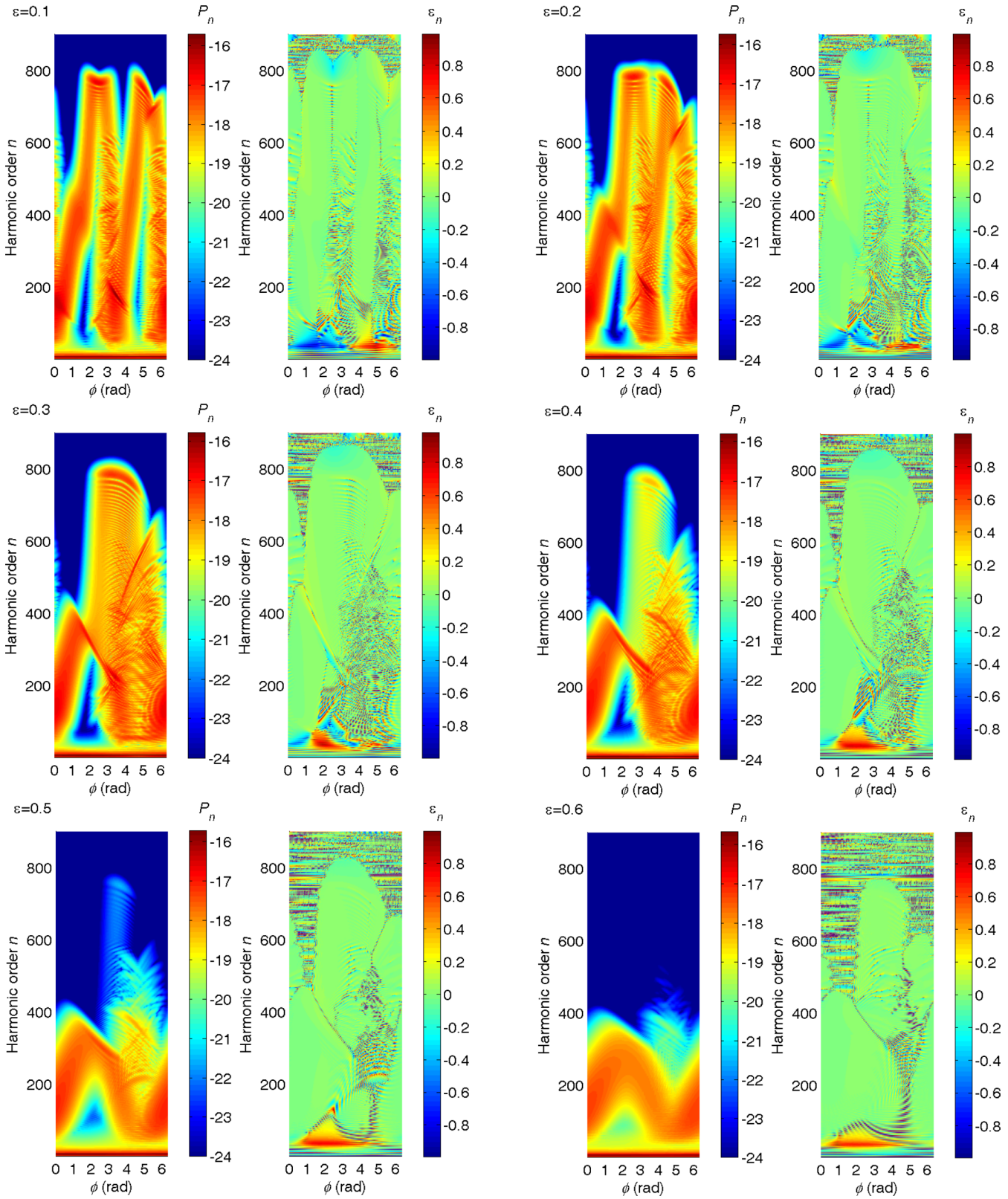

FIG. 3. Same as in Fig. 2 but for the ellipticities $\varepsilon = 0.1, \ldots, 0.6$, as indicated in the upper left corner of each panel.

($\varepsilon = 0.1$). To further explore this, in Fig. 8 we present results for the ellipticity $\varepsilon = 0.01$ (for most practical purposes, this would be a linearly polarized field). In the lower panel of Fig. 8 we show the same results but enlarged for low harmonic orders. The harmonic ellipticities have large positive values for harmonic orders close to the ionization potential of He (the value of I_p/ω is represented by horizontal lines in the right panels) and for particular values of the relative phase.

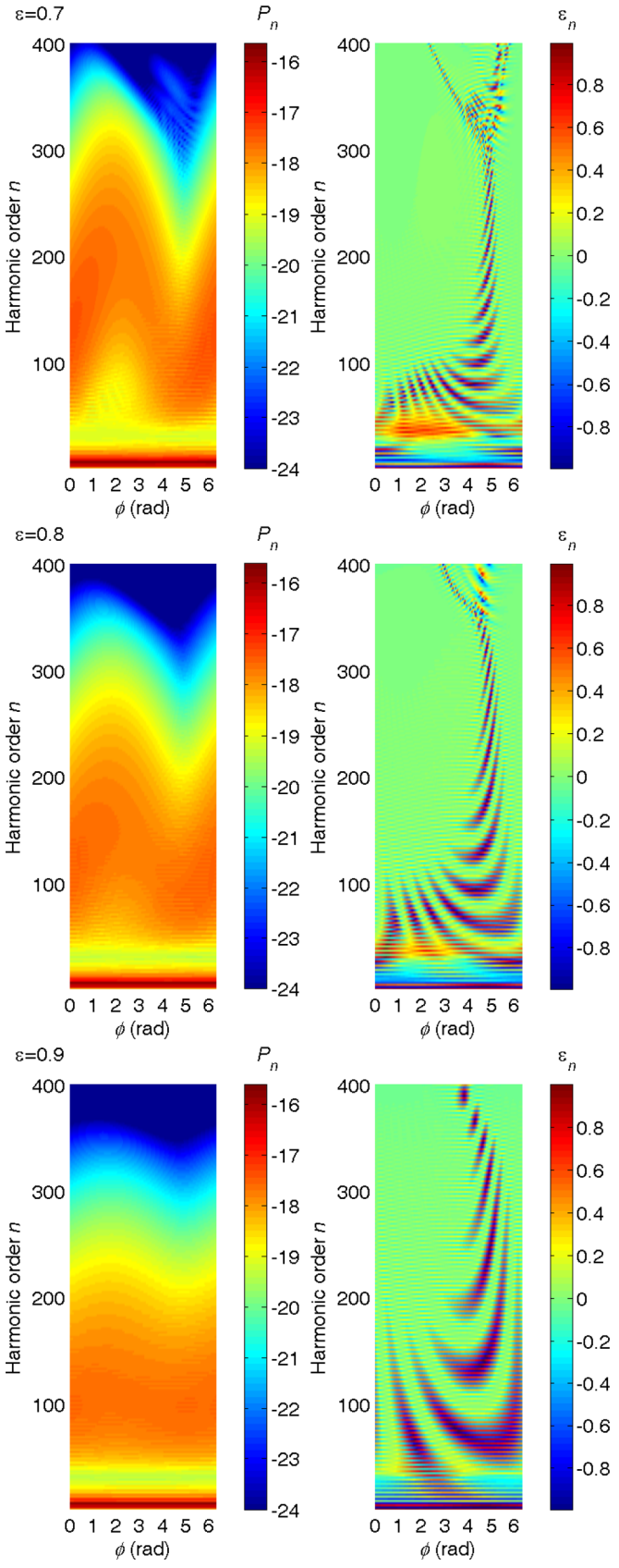

FIG. 4. Same as in Fig. 2 but for the ellipticities $\varepsilon = 0.7, 0.8, 0.9$, as indicated in the upper left corner of each panel.

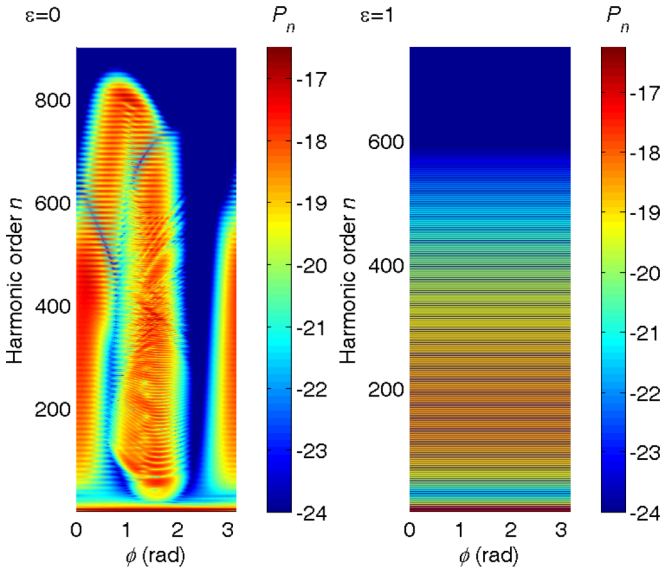

FIG. 5. Logarithm of the harmonic intensity P_n for HHG by He atoms, presented in false colors as functions of the relative phase ϕ (abscissa) between the ω-2ω BEOTC field components and the harmonic order n (ordinate). The component intensities are $E_1^2 = E_2^2 = 5 \times 10^{14}$ W/cm^2 and the fundamental wavelength is 1800 nm. The BEOTC field component ellipticities are equal: $\varepsilon = 0$ (left, OTC), $\varepsilon = 1$ (right, bicircular).

Unfortunately, the corresponding harmonic intensity is rather low for these values. Surprisingly large harmonic ellipticities for very low BEOTC field ellipticity were also reported in a recent paper [66].

The question is why it is that the harmonic ellipticity can be so large for small values of the BEOTC field ellipticity. For $\varepsilon = 0$ the former field reduces to the OTC field and the time-dependent dipole satisfies the relations $d_x(t + T/2) = -d_x(t)$, $d_y(t + T/2) = d_y(t)$, from which it follows that the emitted odd harmonics are polarized in the x direction, while the even harmonics are polarized in the y direction. Using the relation $T_{n\pm} = (T_{nx} \mp iT_{ny})/\sqrt{2}$ it follows that for the OTC field we have $T_{n+} = (-1)^{n+1} T_{n-}$ so that $|T_{n+}|^2 = |T_{n-}|^2$, $\xi_n = (|T_{n+}|^2 - |T_{n-}|^2)/(|T_{n+}|^2 + |T_{n-}|^2) = 0$, and $\varepsilon_n = 0$. For $\varepsilon \neq 0$ the above relations no longer hold and the harmonics are elliptically polarized. In the strong-field approximation the time-dependent dipole can be represented as an integral over the travel time τ [29]:

$$\mathbf{d}(t) = \int_0^\infty d\tau \left(\frac{2\pi}{i\tau}\right)^{3/2} \frac{\partial \psi_0(\mathbf{q})}{\partial \mathbf{q}}|_{\mathbf{q}=\mathbf{k}_s+\mathbf{A}(t)} \times \langle \mathbf{k}_s + \mathbf{A}(t_0)|\mathbf{r} \cdot \mathbf{E}(t_0)|\psi_0\rangle e^{iS(t,\tau)}, \quad (13)$$

where $\mathbf{A}(t) = -\int^t dt' \mathbf{E}(t')$, $\mathbf{k}_s = -\int_{t_0}^t dt' \mathbf{A}(t')/\tau$ is the stationary momentum, $t_0 = t - \tau$, S is the action, and ψ_0 is the atomic ground-state wave function. For the He atom we have $\partial\psi_0(\mathbf{q})/\partial\mathbf{q} = \hat{\mathbf{e}}_\mathbf{q} \partial\psi_0(\mathbf{q})/\partial q$, where, in spherical coordinates, $\hat{\mathbf{e}}_\mathbf{q} = \mathbf{q}/|\mathbf{q}| = (\cos\phi_\mathbf{q}, \sin\phi_\mathbf{q}, 0)$. Taking into account that $\hat{\mathbf{e}}_\pm \cdot \hat{\mathbf{e}}_\pm = 0$, $\hat{\mathbf{e}}_\pm \cdot \hat{\mathbf{e}}_\mp = 1$, we obtain

$$T_{n\pm} = \mathbf{T}_n \cdot \hat{\mathbf{e}}_\mp \propto \int dt \int d\tau f(t,\tau) e^{\mp i\phi_\mathbf{q}(t,\tau)}, \quad (14)$$

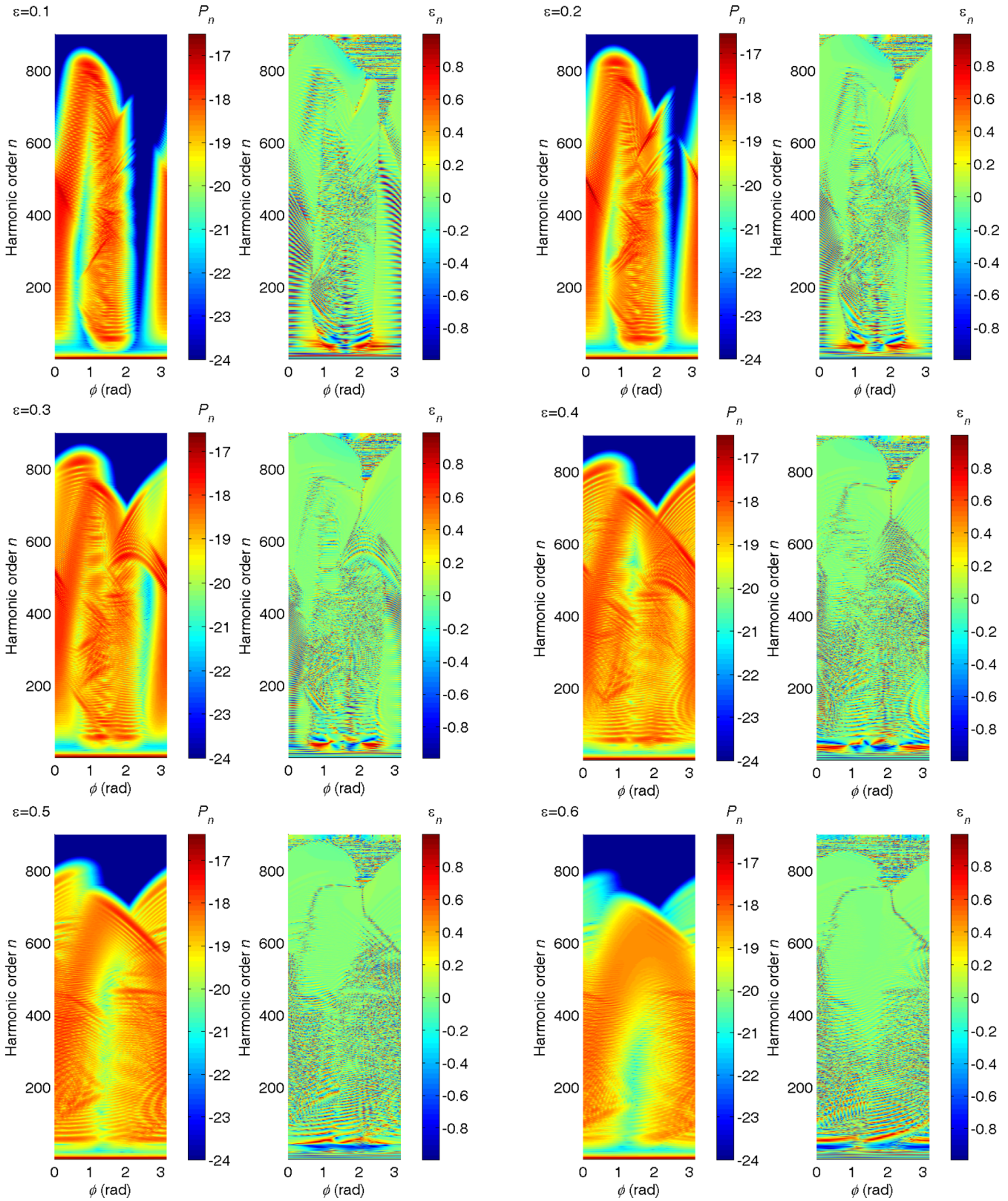

FIG. 6. Same as in Fig. 3 but for the the ω-2ω BEOTC field and the relative phase $\phi \in [0, \pi]$. The ellipticities $\varepsilon = 0.1, \ldots, 0.6$ are indicated in the upper left corner of each panel.

where $f(t, \tau)$ is the same function both for T_{n+} and T_{n-}. Since in the exponent we have $\mp i\phi_{\mathbf{q}}(t, \tau)$ and since we integrate over t and τ, even a small ellipticity ε can lead to a large difference between the T_{n+} and T_{n-} matrix elements, which gives

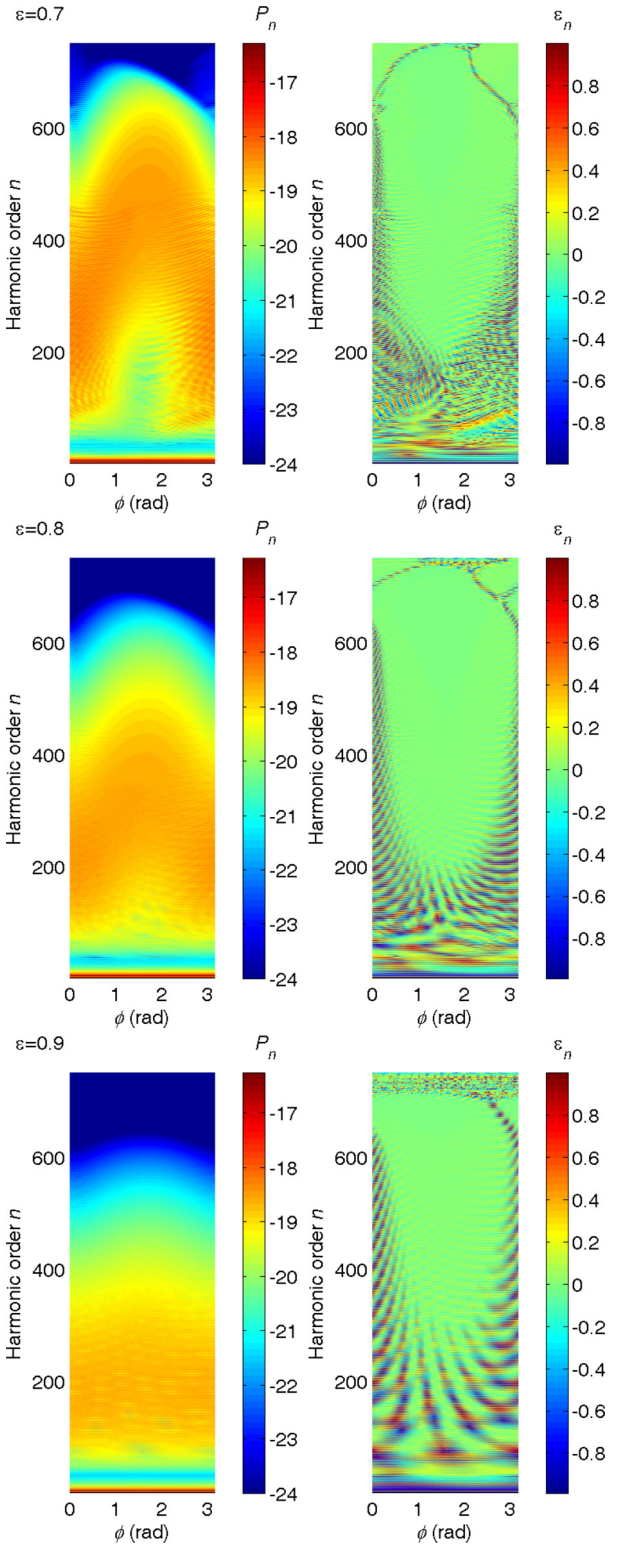

FIG. 7. Same as in Fig. 6 but for the ellipticities $\varepsilon = 0.7, 0.8, 0.9$, as indicated in the upper left corner of each panel.

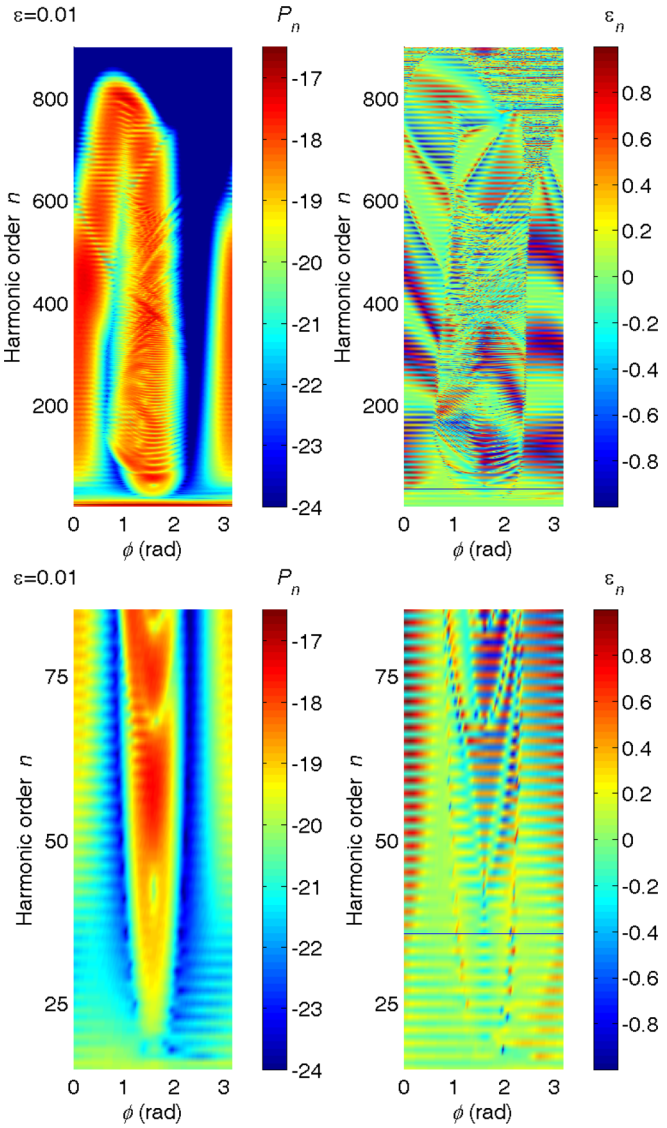

FIG. 8. Logarithm of the harmonic intensities P_n (left) and the ellipticities ε_n (right). The laser and atomic parameters are the same as in Fig. 6 except for the ellipticity, which is $\varepsilon = 0.01$.

a large value of $\xi_n = (|T_{n+}|^2 - |T_{n-}|^2)/(|T_{n+}|^2 + |T_{n-}|^2)$. In Fig. 9 we display the degree of circular polarization ξ_n as a function of the harmonic order for various small values of the ellipticity ε. Even for ε as small as 10^{-5} (magenta line), ξ_n can be different from zero. This is especially pronounced for harmonics close to the cutoff. With increasing ε, ξ_n becomes larger. It oscillates between large positive values (for n odd) and large negative values (for n even), forming two curves in the n-ξ_n plane. These two curves are not symmetric with respect to the n axis. For practical applications, it is important that for a wide range of harmonic orders the value of $|\xi_n|$ is very close to 1, i.e., the corresponding harmonics are nearly circularly polarized.

In Fig. 10 we show, in false-color presentation, how the parameter ξ_n changes with the laser field ellipticity $0 \leqslant \varepsilon \leqslant 0.5$ (abscissa) and the harmonic order (ordinate). We see that, for fixed ellipticity larger than those presented in Fig. 9, the parameter ξ_n has an oscillatory structure. The period of oscillations decreases with increasing ε. We also see that for ellipticities between 0.36 and 0.49 and low harmonic order (close to the value $I_p/\omega = 35.7$) there is a region in which the parameter ξ_n is close to 1. We observed a similar effect in Fig. 8. The explanation why the harmonic ellipticity can be large for

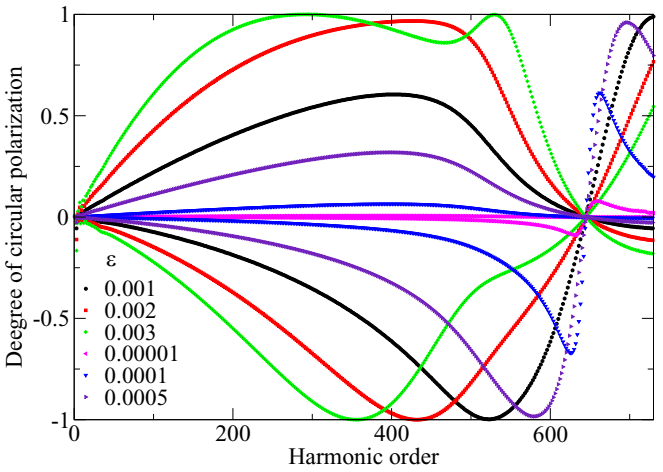

FIG. 9. Degree of circular polarization ξ_n as a function of the harmonic order n for values of the laser field ellipticity denoted in the legend. For given ellipticity, there are two curves: odd (even) harmonics correspond to (for $n \lesssim 640$) a positive (negative) degree of polarization. The component intensities are $E_1^2 = E_2^2 = 5 \times 10^{14}$ W/cm^2, the fundamental wavelength is 1800 nm, the relative phase is $\phi = 0$, and the atom is He.

low harmonic order follows from the formula which expresses the degree of circular polarization via the T-matrix element of the HHG process: $\xi_n = \mathrm{Im}\,(2T_{nx}^* T_{ny})/|T_n|^2 = 2\varepsilon_n/(1+\varepsilon_n^2)$. The imaginary part of the T-matrix element can be large for low harmonic order when the harmonic photon energy is close to the ionization potential, which implies that the value of ξ_n can also be large as shown in Figs. 8 and 10.

Our paper is a follow-up of Ref. [31], where we considered harmonic generation by OTC fields (both fields being linearly polarized). This paper also exhibited surprising results regarding the shape of the harmonic spectra and their polarization (for the frequency ratio 1:3). We were able to explain the spectral shape in terms of the simple-man model

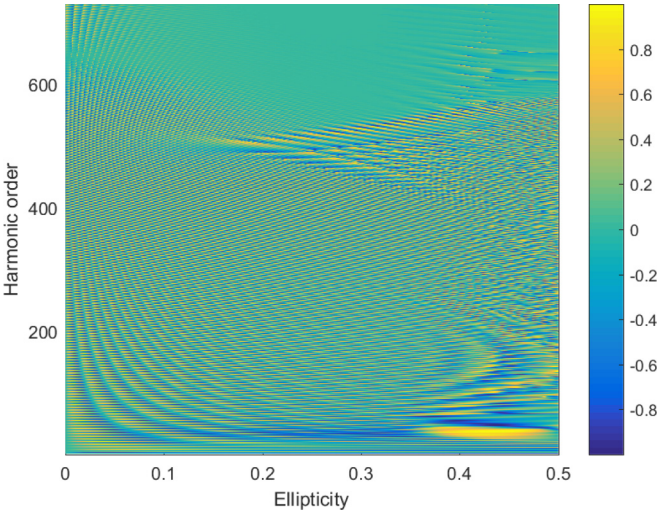

FIG. 10. Degree of circular polarization ξ_n presented in false colors as a function of the laser ellipticity and harmonic order. Other parameters are the same as in Fig. 9.

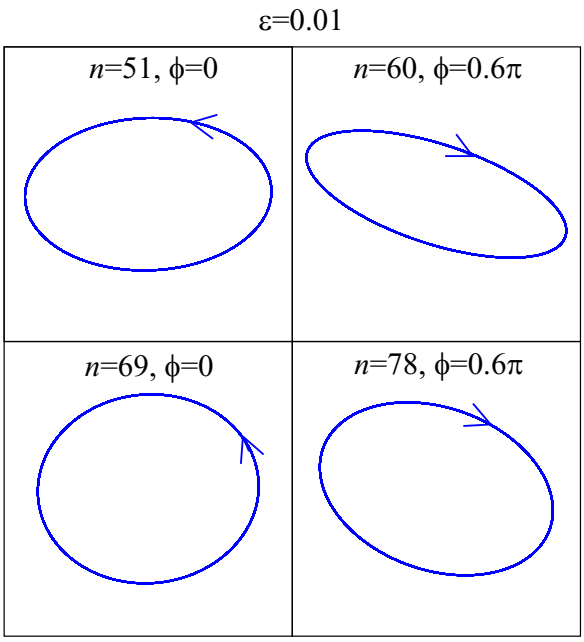

FIG. 11. Examples of the harmonic field calculated using the results of Fig. 8. The corresponding values of the harmonic order and the relative phase are denoted in each panel.

and quantum orbits. However, we made no attempt to explain the polarization in terms of models. In the current paper, we consider BEOTC fields. Again, the results are surprising, especially the fact that very small ellipticities of the driving fields are sufficient, in some cases, to generate harmonics with large ellipticity. We provide some arguments that explain how this can formally come about. But again we are unable to provide an intuitive explanation of the harmonic polarization. The quantum-orbit model appears to be not capable of dealing with the polarization of the harmonics; at least, it has to our knowledge never been employed for this purpose.

Finally, in Fig. 11 we present a few examples of the harmonic field, defined as $\mathrm{Re}\,\mathbf{E}_n$, for various values of the harmonic order and relative phase. Obviously, the harmonic field is close to circular in all examples presented.

C. Results for the ω-2ω BEOTC field and 800 nm

Finally, we analyze the harmonic intensity and the harmonic ellipticity as functions of the relative phase and ellipticity of the ω-2ω BEOTC field, for HHG by a He atom, equal component intensities $E_1^2 = E_2^2 = 4 \times 10^{14}$ W/cm^2 and the fundamental wavelength of 800 nm. The corresponding results are presented in Figs. 12, 13, and 14. Figure 12 illustrates a "shift" of the selection rules. For Figs. 13 and 14 the harmonic orders are fixed to the values $n = 38$, 39, 40, and 41, as indicated in each panel.

According to the selection rules for the bicircular field ($\varepsilon = 1$), the harmonics $n = 3q$, $q = 1, 2, \ldots$, should be missing. Indeed, this is clearly visible in the top panel of Fig. 12, where the results for the bicircular field ($\varepsilon = 1$) are presented. For example, the harmonic intensity P_{39} is zero, with the harmonic $n = 39$ indicated by a dotted blue line. In addition, the polar diagram of the corresponding electric-field vector is

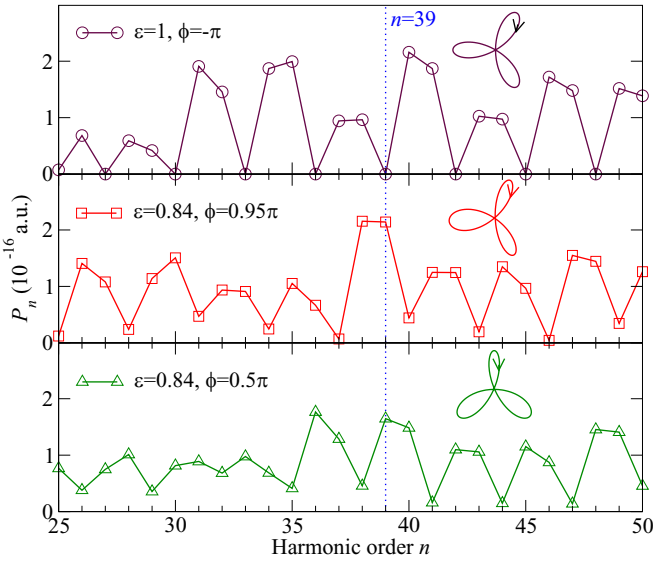

FIG. 12. Harmonic intensity P_n as a function of the harmonic order n for HHG by He atoms exposed to the ω-2ω BEOTC field with equal component intensities $E_1^2 = E_2^2 = 4 \times 10^{14}$ W/cm^2 and the fundamental wavelength of 800 nm. The values of the ellipticity ε and the relative phase ϕ between the field components are denoted in each panel. The top panel corresponds to a bicircular field, for which the harmonic intensity is independent of ϕ. The middle and bottom panels correspond to two different cases of the BEOTC field. In each panel a polar diagram of the electric-field vector of the corresponding field is presented. The harmonic $n = 39$ (for which the harmonic intensity is zero for bicircular field, according to the selection rules) is denoted by a vertical dotted blue line.

presented. The arrow indicates how the field develops with increasing time. For the bicircular field the harmonic intensity does not depend on the value of the relative phase ϕ. We have chosen the value $\phi = -\pi$ for which the electric-field vector resembles the one of the BEOTC field with $\varepsilon = 0.84$ and $\phi = 0.95\pi$. The results for this BEOTC field are shown in the middle panel. One can see that in this case the intensity of the "forbidden" harmonic $n = 39$ has a maximum, while the intensity of the next harmonic $n = 40$ now exhibits a minimum. Comparing the spectra for $\varepsilon = 1$ and $\varepsilon = 0.84$ it looks like they are shifted by one harmonic order. However, this is only approximate so that the "shifted selection rules" are rather propensity rules. Moreover, they depend on the value of the relative phase. In the bottom panel of Fig. 12 corresponding spectra are presented for the relative phase $\phi = 0.5\pi$. We observe a shift of the selection rules by one more unit; i.e., the minimum now occurs at the harmonic $n = 41$. Alternatively, we can say that the spectrum has shifted by one unit to the left, compared with the bicircular case. It is interesting that our results are in agreement with the experiment [67] (see also Ref. [68]).

For a closer illustration of this phenomenon, in Fig. 13 we present the harmonic intensities (upper panels) and ellipticities (lower panels) for fixed harmonic orders $n = 38$, 39, 40, and 41, presented in false colors as functions of the relative phase and the ellipticity. In the upper row, second panel from the left, we see that for $\varepsilon = 1$ the harmonic intensity P_{39} is zero. Also in accordance with the selection rules, the ellipticities of the harmonics $n = 38$ and $n = 41$ are -1, while for $n = 40$ we have $\varepsilon_{40} = +1$. This is visible in the lower row of Fig. 13 for $\varepsilon = 1$. However, depending on the value of the relative phase ϕ, already a very small decrease of the ellipticity can completely change this picture: for $n = 39$ and for ε between 0.8 and 0.9, the harmonic intensity can be high and the ellipticity can be close to -1. In addition, the $n = 38$ harmonic intensity is high and the ellipticity goes from -1 for $\varepsilon = 1$ to $+1$ for ε close to 0.8. On the other hand, the $(n = 40)$-harmonic intensity decreases, while the $(n = 41)$-harmonic ellipticity goes from -1 to $+1$ when the ellipticity decreases from $\varepsilon = 1$ to $\varepsilon = 0.8$. All in all, when the driving ellipticity decreases to values between 0.9 to 0.8 so that the driving field just barely starts to deviate from the bicircular shape, the properties of the harmonics change

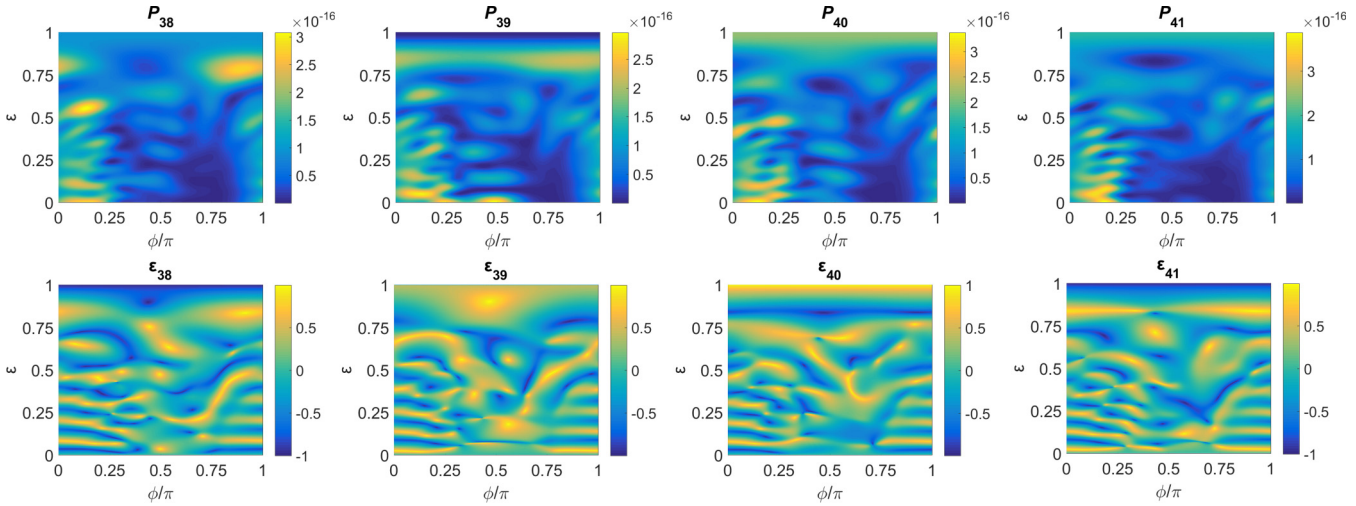

FIG. 13. Harmonic intensities P_n (upper panels) and ellipticities ε_n (lower panels) for $n = 38$, 39, 40, and 41, presented in false colors as functions of the relative phase ϕ (abscissa) between the ω-2ω BEOTC field components and the ellipticity ε (ordinate). Other parameters are as in Fig. 12.

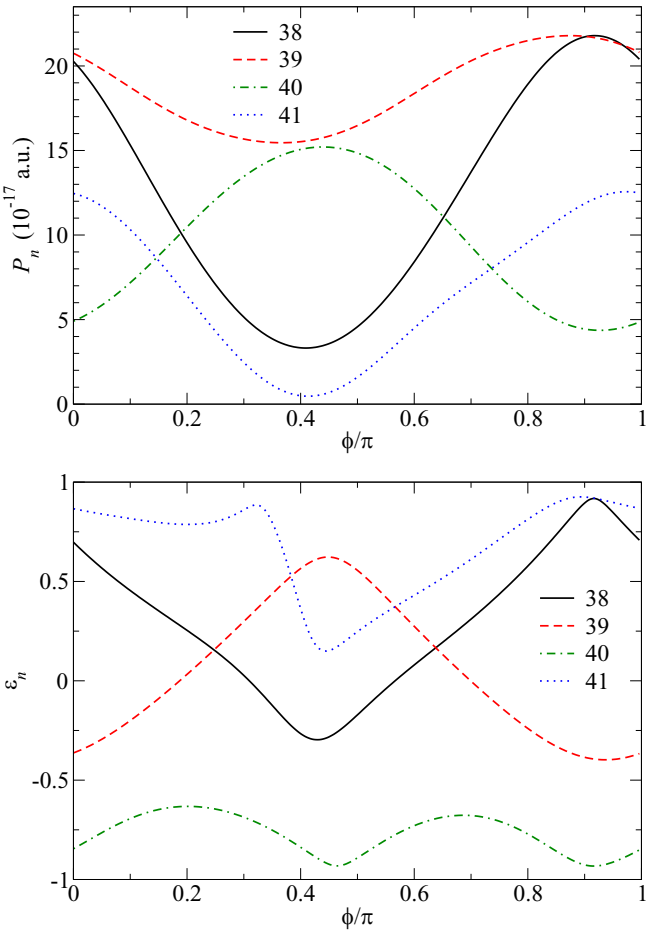

FIG. 14. Harmonic intensities P_n (upper panel) and ellipticities ε_n (lower panel), for the harmonic orders $n = 38$, 39, 40, and 41, as denoted in the legend. The BEOTC field ellipticity is $\varepsilon = 0.84$ and other parameters are as in Fig. 12.

drastically. High-harmonic intensities become low and the harmonic helicities change sign.

For a still closer look, in Fig. 14 we present results for fixed value of the ellipticity: $\varepsilon = 0.84$. We see that for $n = 38$ (black solid lines) and the phase $\phi = 0.915\pi$ the harmonic intensity has a maximum and the harmonic ellipticity is $\varepsilon_{38} = 0.918$, almost opposite to the one for the bicircular field ($\varepsilon_{38} = -1$ for $\varepsilon = 1$). For the 39th harmonic the harmonic ellipticity is maximal ($\varepsilon_{39} = 0.623$) for the phase $\phi = 0.449\pi$. For $n = 40$ ($n = 41$) the harmonic ellipticity is close to -1 ($+1$) for two values of the relative phase: $\phi = 0.465\pi$ and 0.915π (0.324π and 0.886π).

In Fig. 1 we have displayed the electric-field vectors of the high-harmonic fields defined as $\mathrm{Re}\,\mathbf{E}_n(t)$ for $n = 38$, 39, 40, and 41, corresponding to the parameters $\varepsilon = 0.84$ and $\phi = 0.92\pi$ of Fig. 14. For the harmonics $n = \{38, 39, 40, 41\}$ the corresponding ellipticities are $\varepsilon_n = \{0.92, -0.39, -0.93, 0.92\}$. This is an almost complete reversal from the case of the bicircular field ($\varepsilon = 1$), where the corresponding ellipticities are $\varepsilon_n = \{-1, \text{undefined}, +1, -1\}$.

IV. CONCLUSIONS

Having in mind that it is nowadays possible to generate strong bi-elliptical orthogonally polarized driving laser pulses, we explored in detail how the HHG process depends on the parameters of these fields. We considered the ω-2ω and ω-3ω field combinations and varied the relative phase ϕ between the two driving-field components as well as their ellipticity from $\varepsilon = 0$ to $\varepsilon = 1$. The results for the ω-3ω field for $-\varepsilon$ and ϕ can be obtained from those for ε and $\phi + \pi$. For the ω-2ω field the results are invariant with respect to $\phi \to \phi + \pi$, while for $\varepsilon \to -\varepsilon$ the harmonic intensity remains the same and the harmonic ellipticity changes sign. These results exhibit various interesting and unexpected features.

Most importantly, we identified the regions of the driving laser field parameters in which the harmonic ellipticity can be very high. For the ω-3ω field, in addition to results previously obtained for the OTC field [31], we found regions of low harmonic order for which the harmonic ellipticity is high. For the ω-2ω field having very low ellipticity ($\varepsilon = 0.01$), we observed that the harmonic ellipticity can be very high. This is very unexpected, since for $\varepsilon = 0$ the emitted harmonics are strictly linearly polarized, owing to rigorous selection rules. Similar observations were very recently reported in Ref. [66]. We explained this by the magnitudes of the nth T-matrix-element components with helicities $+1$ and -1, T_{n+} and T_{n-}, which can become very different even for small driving-field ellipticities (recall that $T_{n+} = T_{n-}$ for the OTC field). In addition, the imaginary part of the T-matrix element becomes large for low harmonic order [close to the atomic ionization potential; the degree of circular polarization is proportional to $\mathrm{Im}\,(2T^*_{nx}T_{ny})$].

Another interesting result is a shift of the known selection rules that hold for a bicircular field (i.e., for the ω-2ω bicircular field the emitted harmonics $n_\pm = 3q_- \pm 1$ have the helicity $\varepsilon_{n\pm} = \pm 1$). We have found a shift of the corresponding harmonic order by one for particular values of the relative phase and for large ellipticities of the BEOTC ω-2ω field. These are not new selection rules but rather propensity rules. They are only approximate (the harmonic ellipticity is not exactly ± 1) and dependent on the relative phase.

The BEOTC field as a function of its ellipticity interpolates between the limiting cases of the linearly polarized two-color (OTC) field for $\varepsilon = 0$ and the bicircular field for $\varepsilon = 1$. Surprisingly, we found that the departure from these two limiting cases occurs very fast. Already a very small ellipticity of, say, $\varepsilon = 0.01$ can generate harmonics with substantial nonzero ellipticity, and a rather small deviation from the bicircular field of, say, $\varepsilon = 0.84$ can completely invalidate the bicircular selection rules. All this depends very strongly on the relative phase between the two driving-field components.

The rapid departure of the harmonic spectrum and ellipticities from the respective limiting case can be experimentally relevant. For example, in Ref. [58] the authors reported high degrees of ellipticity (up to 75%) of the emitted harmonics for an ω-2ω OTC field, in complete violation of the selection rules for this field, which predict linearly polarized harmonics. In light of the above, a possible explanation is that, instead of a pure linearly polarized field they actually had a small nonzero ellipticity. Then, according to our results it is possible

to have a large ellipticity of the harmonics. They utilized these harmonics to measure the x-ray magnetic circular dichroism effect of nickel at the $M_{2,3}$ absorption edge around 67 eV. In Ref. [14] a bicircular field combination was used to generate almost circularly polarized harmonics and to measure the x-ray magnetic circular dichroism at the Fe $M_{2,3}$ absorption edge (54 eV) and the Gd $N_{4,5}$ edge (145 eV) [14]. Gd is a technologically important rare earth metal. Such materials are of wide interest because they are potentially important for next-generation data-storage media using all-optical switching.

In our case, the harmonic order can be much higher than 800, which corresponds to a photon energy of 551 eV (for an 1800-nm laser the photon energy is 0.6888 eV). In Ref. [31] using a 2200-nm midinfrared laser and an ω-3ω OTC field we achieved photon energies above 1200 eV. With the present BEOTC field and for the ω-2ω field combination these energies can be higher. In any case, they can be used to explore, for example, the L edges of manganese (640 eV) and copper (930 eV). Another important result of our investigation is that the relative phase between the two driving-field components affords enormous control of the spectral shape and polarization.

ACKNOWLEDGMENTS

We acknowledge support by the Ministry for Education, Science and Youth, Canton Sarajevo, Bosnia and Herzegovina. We also acknowledge support by the Alexander von Humboldt Foundation.

[1] N. Böwering, T. Lischke, B. Schmidtke, N. Müller, T. Khalil, and U. Heinzmann, Asymmetry in Photoelectron Emission from Chiral Molecules Induced by Circularly Polarized Light, Phys. Rev. Lett. **86**, 1187 (2001).

[2] U. Hergenhahn, E. E. Rennie, O. Kugeler, S. Marburger, T. Lischke, I. Powis, and G. Garcia, Photoelectron circular dichroism in core level ionization of randomly oriented pure enantiomers of the chiral molecule camphor, J. Chem. Phys. **120**, 4553 (2004).

[3] C. Lux, M. Wollenhaupt, T. Bolze, Q. Liang, J. Köhler, C. Sarpe, and T. Baumert, Circular dichroism in the photoelectron angular distributions of camphor and fenchone from multiphoton ionization with femtosecond laser pulses, Angew. Chem. Int. Ed. **51**, 5001 (2012).

[4] A. Ferré, C. Handschin, M. Dumergue, F. Burgy, A. Comby, D. Descamps, B. Fabre, G. A. Garcia, R. Géneaux, L. Merceron, E. Mével, L. Nahon, S. Petit, B. Pons, D. Staedter, S. Weber, T. Ruchon, V. Blanchet, and Y. Mairesse, A table-top ultrashort light source in the extreme ultraviolet for circular dichroism experiments, Nat. Photonics **9**, 93 (2014).

[5] R. Cireasa, A. E. Boguslavskiy, B. Pons, M. C. H. Wong, D. Descamps, S. Petit, H. Ruf, N. Thiré, A. Ferré, J. Suarez, J. Higuet, B. E. Schmidt, A. F. Alharbi, F. Legare, V. Blanchet, B. Fabre, S. Patchkovskii, O. Smirnova, Y. Mairesse, and V. R. Bhardwaj, Probing molecular chirality on a sub-femtosecond timescale, Nat. Phys. **11**, 654 (2015).

[6] S. Beaulieu, A. Comby, B. Fabre, D. Descamps, A. Ferre, G. Garcia, R. Geneaux, F. Legare, L. Nahon, S. Petit, T. Ruchon, B. Pons, V. Blanchet, and Y. Mairesse, Probing ultrafast dynamics of chiral molecules using time-resolved photoelectron circular dichroism, Faraday Discuss. **194**, 325 (2016).

[7] L. Nahon, L. Nag, G. A. Garcia, I. Myrgorodska, U. Meierhenrich, S. Beaulieu, V. Wanie, V. Blanchet, R. Géneaux, and I. Powis, Determination of accurate electron chiral asymmetries in fenchone and camphor in the VUV range: Sensitivity to isomerism and enantiomeric purity, Phys. Chem. Chem. Phys. **18**, 12696 (2016).

[8] R. Hadidi, D. K. Bozanic, G. A. Garcia, and L. Nahon, Electron asymmetries in the photoionization of chiral molecules: Possible astrophysical implications, Adv. Phys. X **3**, 1477530 (2018).

[9] S. Beaulieu, A. Comby, D. Descamps, B. Fabre, G. A. Garcia, R. Géneaux, A. G. Harvey, F. Légaré, Z. Mašín, L. Nahon, A. F. Ordonez, S. Petit, B. Pons, Y. Mairesse, O. Smirnova, and V. Blanchet, Photoexcitation circular dichroism in chiral molecules, Nat. Phys. **14**, 484 (2018).

[10] P. V. Demekhin, A. N. Artemyev, A. Kastner, and T. Baumert, Photoelectron Circular Dichroism with Two Overlapping Laser Pulses of Carrier Frequencies ω and 2ω Linearly Polarized in Two Mutually Orthogonal Directions, Phys. Rev. Lett. **121**, 253201 (2018).

[11] P. Fischer, D.-H. Kim, W. Chao, J. A. Liddle, E. H. Anderson, and D. T. Attwood, Soft X-ray microscopy of nanomagnetism, Mater. Today **9**, 26 (2006).

[12] S. Eisebitt, J. Lüning, W. F. Schlotter, M. Lörgen, O. Hellwig, W. Eberhardt, and J. Stöhr, Lensless imaging of magnetic nanostructures by x-ray spectro-holography, Nature (London) **432**, 885 (2004).

[13] C. Boeglin, E. Beaurepaire, V. Halte, V. Lopez-Flores, C. Stamm, N. Pontius, H. A. Durr, and J. Y. Bigot, Distinguishing the ultrafast dynamics of spin and orbital moments in solids, Nature (London) **465**, 458 (2010).

[14] T. Fan, P. Grychtol, R. Knut, C. Hernández-García, D. D. Hickstein, D. Zusin, C. Gentry, F. J. Dollar, C. A. Mancuso, C. Hogle, O. Kfir, D. Legut, K. Carva, J. L. Ellis, K. Dorney, C. Chen, O. Shpyrko, E. E. Fullerton, O. Cohen, P. M. Oppeneer, D. B. Milošević, A. Becker, A. A. Jaroń-Becker, T. Popmintchev, M. M. Murnane, and H. C. Kapteyn, Bright circularly polarized soft x-ray high harmonics for x-ray magnetic circular dichroism, Proc. Natl. Acad. Sci. USA **112**, 14206 (2015).

[15] O. Kfir, S. Zayko, C. Nolte, M. Sivis, M. Möller, B. Hebler, S. S. P. K. Arekapudi, D. Steil, S. Schäfer, M. Albrecht, O. Cohen, S. Mathias, and C. Ropers, Nanoscale magnetic imaging using circularly polarized high-harmonic radiation, Sci. Adv. **3**, eaao4641 (2017).

[16] J. L. Ellis, K. M. Dorney, D. D. Hickstein, N. J. Brooks, C. Gentry, C. Hernández-García, D. Zusin, J. M. Shaw, Q. L. Nguyen, C. A. Mancuso, G. S. M. Jansen, S. Witte, H. C. Kapteyn, and M. M. Murnane, High harmonics with spatially varying ellipticity, Optica **5**, 479 (2018).

[17] C. T. Chen, Y. U. Idzerda, H.-J. Lin, N. V. Smith, G. Meigs, E. Chaban, G. H. Ho, E. Pellegrin, and F. Sette, Experimental Confirmation of the X-Ray Magnetic Circular Dichroism Sum Rules for Iron and Cobalt, Phys. Rev. Lett. **75**, 152 (1995).

[18] J. B. Kortright and S-K. Kim, Resonant magneto-optical properties of Fe near its $2p$ levels: Measurement and applications, Phys. Rev. B **62**, 12216 (2000).

[19] S. Valencia, A. Gaupp, W. Gudat, H-Ch. Mertins, P. M. Oppeneer, D. Abramsohn, and C. M. Schneider, Faraday rotation spectra at shallow core levels: $3p$ edges of Fe, Co, and Ni, New J. Phys. **8**, 254 (2006).

[20] H. Eichmann, A. Egbert, S. Nolte, C. Momma, B. Wellegehausen, W. Becker, S. Long, and J. K. McIver, Polarization-dependent high-order two-color mixing, Phys. Rev. A **51**, R3414 (1995).

[21] S. Long, W. Becker, and J. K. McIver, Model calculations of polarization-dependent two-color high-harmonic generation, Phys. Rev. A **52**, 2262 (1995).

[22] T. Zuo and A. D. Bandrauk, High-order harmonic generation in intense laser and magnetic fields, J. Nonlinear Opt. Phys. Mater. **04**, 533 (1995).

[23] D. B. Milošević, W. Becker, and R. Kopold, Generation of circularly polarized high-order harmonics by two-color coplanar field mixing, Phys. Rev. A **61**, 063403 (2000).

[24] D. B. Milošević and W. Becker, Attosecond pulse trains with unusual nonlinear polarization, Phys. Rev. A **62**, 011403(R) (2000).

[25] A. Fleischer, O. Kfir, T. Diskin, P. Sidorenko, and O. Cohen, Spin angular momentum and tunable polarization in high-harmonic generation, Nat. Photonics **8**, 543 (2014).

[26] D. B. Milošević, High-order harmonic generation by a bichromatic elliptically polarized field: Conservation of angular momentum, J. Phys. B **48**, 171001 (2015).

[27] D. B. Milošević, Generation of elliptically polarized attosecond pulse trains, Opt. Lett. **40**, 2381 (2015).

[28] L. Medišauskas, J. Wragg, H. van der Hart, and M. Yu. Ivanov, Generating Isolated Elliptically Polarized Attosecond Pulses Using Bichromatic Counterrotating Circularly Polarized Laser Fields, Phys. Rev. Lett. **115**, 153001 (2015).

[29] D. B. Milošević, Circularly polarized high harmonics generated by a bicircular field from inert atomic gases in the p state: A tool for exploring chirality-sensitive processes, Phys. Rev. A **92**, 043827 (2015).

[30] C. Chen, Z. Tao, C. Hernández-García, P. Matyba, A. Carr, R. Knut, O. Kfir, D. Zusin, C. Gentry, P. Grychtol, O. Cohen, L. Plaja, A. Becker, A. Jaron-Becker, H. Kapteyn, and M. Murnane, Tomographic reconstruction of circularly polarized high-harmonic fields: 3D attosecond metrology, Sci. Adv. **2**, e1501333 (2016).

[31] D. B. Milošević and W. Becker, X-ray harmonic generation by orthogonally polarized two-color fields: Spectral shape and polarization, Phys. Rev. A **100**, 031401(R) (2019).

[32] M. D. Perry and J. K. Crane, High-order harmonic emission from mixed fields, Phys. Rev. A **48**, R4051(R) (1993).

[33] I. J. Kim, C. M. Kim, H. T. Kim, G. H. Lee, Y. S. Lee, J. Y. Park, D. J. Cho, and C. H. Nam, Highly Efficient High-Harmonic Generation in an Orthogonally Polarized Two-Color Laser Field, Phys. Rev. Lett. **94**, 243901 (2005).

[34] C. M. Kim, I. J. Kim, and C. H. Nam, Generation of a strong attosecond pulse train with an orthogonally polarized two-color laser field, Phys. Rev. A **72**, 033817 (2005).

[35] L. Brugnera, D. J. Hoffmann, T. Siegel, F. Frank, A. Zaïr, J. W. G. Tisch, and J. P. Marangos, Trajectory Selection in High Harmonic Generation by Controlling the Phase Between Orthogonal Two-Color Fields, Phys. Rev. Lett. **107**, 153902 (2011).

[36] C. M. Kim and C. H. Nam, Selection of an electron path of high-order harmonic generation in a two-colour femtosecond laser field, J. Phys. B **39**, 3199 (2006).

[37] L. Brugnera, F. Frank, D. J. Hoffmann, R. Torres, T. Siegel, J. G. Underwood, E. Springate, C. Froud, E. I. C. Turcu, J. W. G. Tisch, and J. P. Marangos, Enhancement of high harmonics generated by field steering of electrons in a two-color orthogonally polarized laser field, Opt. Lett. **35**, 3994 (2010).

[38] H. Niikura, H. J. Wörner, D. M. Villeneuve, and P. B. Corkum, Probing the Spatial Structure of a Molecular Attosecond Electron Wave Packet Using Shaped Recollision Trajectories, Phys. Rev. Lett. **107**, 093004 (2011).

[39] M. Murakami, O. Korobkin, and M. Horbatsch, High-harmonic generation from hydrogen atoms driven by two-color mutually orthogonal laser fields, Phys. Rev. A **88**, 063419 (2013); **95**, 059909(E) (2017).

[40] D. J. Hoffmann, C. Hutchison, A. Zaïr, and J. P. Marangos, Control of temporal mapping and harmonic intensity modulation using two-color orthogonally polarized fields, Phys. Rev. A **89**, 023423 (2014).

[41] Y. Zheng, H. Diao, Z. Zeng, X. Ge, R. Li, and Z. Xu, Manipulating electron-ion recollision in a midinfrared laser field, Phys. Rev. A **92**, 033417 (2015).

[42] G. Li, Y. Zheng, X. Ge, Z. Zeng, and R. Li, Frequency modulation of high-order harmonic generation in an orthogonally polarized two-color laser field, Opt. Express **24**, 18685 (2016).

[43] P. Wei, J. Miao, Z. Zeng, C. Li, X. Ge, R. Li, and Z. Xu, Selective Enhancement of a Single Harmonic Emission in a Driving Laser Field with Subcycle Waveform Control, Phys. Rev. Lett. **110**, 233903 (2013).

[44] A. S. Emelina, M. Yu. Emelin, R. A. Ganeev, M. Suzuki, H. Kuroda, and V. V. Strelkov, Two-color high-harmonic generation in plasmas: Efficiency dependence on the generating particle properties, Opt. Express **24**, 13971 (2016).

[45] R. A. Ganeev, S. Odžak, D. B. Milošević, M. Suzuki, and H. Kuroda, Resonance enhancement of harmonics in metal plasmas using tunable mid-infrared pulses, Laser Phys. **26**, 075401 (2016).

[46] D. Shafir, H. Soifer, B. D. Bruner, M. Dagan, Y. Mairesse, S. Patchkovskii, M. Y. Ivanov, O. Smirnova, and N. Dudovich, Resolving the time when an electron exits a tunnelling barrier, Nature (London) **485**, 343 (2012).

[47] D. Shafir, Y. Mairesse, D. Villeneuve, P. B. Corkum, and N. Dudovich, Atomic wavefunctions probed through strong-field light-matter interaction, Nat. Phys. **5**, 412 (2009).

[48] D. Shafir, Y. Mairesse, H. J. Wörner, K. Rupnik, D. M. Villeneuve, P. B. Corkum, and N. Dudovich, Probing the symmetry of atomic wavefunctions from the point of view of strong field-driven electrons, New J. Phys. **12**, 073032 (2010).

[49] H. Niikura, N. Dudovich, D. M. Villeneuve, and P. B. Corkum, Mapping Molecular Orbital Symmetry on High-Order

Harmonic Generation Spectrum Using Two-Color Laser Fields, Phys. Rev. Lett. **105**, 053003 (2010).

[50] G. Laurent, W. Cao, H. Li, Z. Wang, I. Ben-Itzhak, and C. L. Cocke, Attosecond Control of Orbital Parity Mix Interferences and the Relative Phase of Even and Odd Harmonics in an Attosecond Pulse Train, Phys. Rev. Lett. **109**, 083001 (2012).

[51] T. S. Sarantseva, M. V. Frolov, N. L. Manakov, M. Yu. Ivanov, and A. F. Starace, Harmonic generation spectroscopy with a two-colour laser field having orthogonal linear polarizations, J. Phys. B **46**, 231001 (2013).

[52] M. V. Frolov, N. L. Manakov, T. S. Sarantseva, A. A. Silaev, N. V. Vvedenskii, and A. F. Starace, Control of threshold enhancements in harmonic generation by atoms in a two-color laser field with orthogonal polarizations, Phys. Rev. A **93**, 023430 (2016).

[53] C. Zhai, X. Zhang, X. Zhu, L. He, Y. Zhang, B. Wang, Q. Zhang, P. Lan, and P. Lu, Single-shot molecular orbital tomography with orthogonal two-color fields, Opt. Express **26**, 2775 (2018).

[54] E. Bordo, O. Neufeld, O. Kfir, A. Fleischer, and O. Cohen, Spectroscopy of atomic orbital sizes using bi-elliptical high-order harmonic generation, Phys. Rev. A **100**, 043419 (2019).

[55] X. Liu, X. Zhu, L. Li, Y. Li, Q. Zhang, P. Lan, and P. Lu, Selection rules of high-order-harmonic generation: Symmetries of molecules and laser fields, Phys. Rev. A **94**, 033410 (2016).

[56] B. Zhang and M. Lein, High-order harmonic generation from diatomic molecules in an orthogonally polarized two-color laser field, Phys. Rev. A **100**, 043401 (2019).

[57] C. Ruiz, D. J. Hoffmann, R. Torres, L. E. Chipperfield, and J. P. Marangos, Control of the polarization of attosecond pulses using a two-color field, New J. Phys. **11**, 113045 (2009).

[58] G. Lambert, B. Vodungbo, J. Gautier, B. Mahieu, V. Malka, S. Sebban, P. Zeitoun, J. Luning, J. Perron, A. Andreev, S. Stremoukhov, F. Ardana-Lamas, A. Dax, C. P. Hauri, A. Sardinha, and M. Fajardo, Towards enabling femtosecond helicity-dependent spectroscopy with high-harmonic sources, Nat. Commun. **6**, 6167 (2015).

[59] S. M. Njoroge, H. Yuan, K. Dickson, Q. Zhang, and P. Lan, Control of the polarization direction of isolated attosecond pulses using inhomogeneous two-color fields, Sci. Rep. **9**, 18582 (2019).

[60] Y. Yu, X. Song, Y. Fu, R. Li, Y. Cheng, and Z. Xu, Theoretical investigation of single attosecond pulse generation in an orthogonally polarized two-color laser field, Opt. Express **16**, 686 (2008).

[61] J. J. Xu, Isolated short attosecond pulse generation in an orthogonally polarized multicycle chirped laser field, Phys. Rev. A **83**, 033823 (2011).

[62] G. Li, Y. Zheng, Z. Zeng, and R. Li, Intense keV IAP generation by orthogonally polarized multicycle midinfrared two-color laser fields, Chin. Opt. Lett. **15**, 071901 (2017).

[63] O. Neufeld, D. Podolsky, and O. Cohen, Floquet group theory and its application to selection rules in harmonic generation, Nat. Commun. **10**, 405 (2019).

[64] T. S. Sarantseva, M. V. Frolov, N. L. Manakov, A. A. Silaev, A. A. Romanov, N. V. Vvedenskii, and A. F. Starace, Attosecond-pulse metrology based on high-order harmonic generation, Phys. Rev. A **101**, 013402 (2020).

[65] A. J. Uzan, H. Soifer, O. Pedatzur, A. Clergerie, S. Larroque, B. D. Bruner, B. Pons, M. Ivanov, O. Smirnova, and N. Dudovich, Spatial molecular interferometry via multidimensional high-harmonic spectroscopy, Nat. Photonics **14**, 188 (2020).

[66] E. Bordo, O. Kfir, S. Zayko, O. Neufeld, A. Fleischer, C. Ropers, and O. Cohen, Interlocked attosecond pulse trains in slightly bi-elliptical high harmonic generation, J. Phys. Photonics **2**, 034005 (2020).

[67] O. Kfir, S. Zayko, C. Nolte, S. Mathias, O. Cohen, and C. Ropers, Attosecond-precision coherent control of electron recombination in the polarization plane, in *Proceedings of the Conference on Lasers and Electro-Optics, San Jose, CA, 2017* (Optical Society of America, Washington, DC, 2017).

[68] S. Zayko, O. Kfir, E. Bordo, A. Fleischer, O. Cohen, and C. Ropers, A dynamical symmetry triad in high-harmonic generation revealed by attosecond recollision control, New J. Phys. **22**, 053017 (2020).

[69] We are using the definition introduced in Ref. [21]. Notice that our definition of left and right circular polarization assumes the point of view of the source for a laser field propagating along the positive z direction. This definition is used by quantum physicists and also by the engineering community and radio astronomers. However, many optics textbooks use the point of view of the receiver for definition of the polarization. In this case, we would have $\hat{\mathbf{e}}_{\pm} = \mp(\hat{\mathbf{e}}_x \pm i\hat{\mathbf{e}}_y)/\sqrt{2}$.

[70] S. Odžak and D. B. Milošević, Ellipticity and the offset angle of high harmonics generated by homonuclear diatomic molecules, J. Phys. B **44**, 125602 (2011).